American Mineralogist, Volume 68, pages 981–988, 1983

Hydrothermal synthesis of goethite–rutile intergrowth structures and their relationship to pseudorutile

IAN E. GREY, CHRISTINA LI AND JOHN A. WATTS

CSIRO Division of Mineral Chemistry
P.O. Box 124, Port Melbourne, Victoria 3207, Australia

Abstract

Hydrothermal crystallization of a series of mixed iron and titanium oxide coprecipitates at 2.2 kbar and at temperatures in the range 150–260°C produced single-phase pseudorutile-related products for the composition range $0.3 \leq Ti/(Ti+Fe) \leq 0.6$. The samples were characterized using thermal analysis (DTA/DTG) and X-ray powder diffraction (XRD) techniques, as being poorly ordered unit-cell intergrowths of iron oxyhydroxide (goethite type) and titanium oxide (rutile type). A parallel study on natural pseudorutile showed that the mineral has very similar properties to the synthetic phases and that it should properly be considered as an oxyhydroxide mineral rather than as an oxide or oxide-hydrate as it has been previously described. Its structure comprises a statistical distribution of twin-variants of a goethite–rutile intergrowth structure in microdomains of average dimension 40–50Å.

Introduction

The mineral pseudorutile is ubiquitous in heavy mineral beach sand deposits as an intermediate alteration product of ilmenite (Temple, 1966). Commercial ilmenite concentrates commonly contain up to 60 weight percent pseudorutile and in Australia alone, it is estimated that more than 300,000 tons of the mineral are exported annually in feedstocks to TiO_2 pigment plants.

In spite of its industrial importance, pseudorutile remains relatively poorly characterized. Its structure is highly disordered (Grey and Reid, 1975) and its composition is variable. Temple (1966) reported that the mineral has a composition approximating to $Fe_2Ti_3O_9$, whereas Dyadchenko and Khatuntseva (1960) assigned a variable composition range to the intermediate alteration phase (termed arizonite (Palmer, 1909) by the Russian workers), $Fe_2O_3 \cdot nTiO_2 \cdot mH_2O$ with $1 < m < 2$ and $3 < n < 5$. Gevorkyan and Tananayev (1964) carried out chemical analyses on altered ilmenites with TiO_2 contents in the range 51.8 to 94.0 wt.% and observed an inverse correlation between iron content and water content. Within the pseudorutile composition range (60–71 wt.% TiO_2 according to the above formula), the water content increased from ~2 to 4.5 wt.% with decreasing iron oxide content. Gevorkyan and Tananayev proposed that the intermediate alteration phases comprised mixtures of TiO_2 with iron hydroxides.

One of the main difficulties in characterizing pseudorutile in altered ilmenites is that it is poorly crystalline and invariably intimately mixed on a very fine scale with rutile, ilmenite and other minor alteration phases. There have been several reported attempts to synthesize the pure compound. (Gmelin, 1932; Pesce, 1931; Ernst, 1943.) Karkhanavala and Momin (1959) reported the formation of pseudorutile mixed with anatase and hematite by hydrothermal synthesis at 300°C and 0.083 kbar. Recently, Fitzpatrick, Le Roux and Schwertmann (1978) studied the crystallization of mixed iron and titanium oxide coprecipitates after ageing at 70°C and pH 5.5 for 70 days. They reported the formation of single-phase products with X-ray powder patterns resembling those of natural pseudorutiles for compositions containing 20–30 wt.% TiO_2 ($Ti/(Ti+Fe)$ atomic ratio = 0.2–0.3). These compositions are well outside the reported range for natural pseudorutiles (Dyadchenko and Khatuntseva, 1960). Compositions with higher TiO_2 contents gave two-phase mixtures with anatase whereas those with lower TiO_2 content contained goethite.

We have extended the type of study carried out by Fitzpatrick *et al.* (1978) to hydrothermal crystallization of mixed oxide coprecipitates and find that single-phase compositions with pseudorutile-like X-ray powder patterns may be prepared for TiO_2 contents in the range 30–60 wt.% at a pressure of 2.2 kbar and at temperatures in the range 150–260°C. We report here the preparation of these phases and their characterization using X-ray diffraction and DTA/DTG techniques, and compare the properties of the synthetic phases with those of natural pseudorutile.

Experimental

A sample of carefully purified natural pseudorutile from a South Australian locality was supplied by the Australian Mineral Development Laboratories. A full

0003–004X/83/0910–0981$02.00

description of this sample has been reported by Larrett and Spencer (1971) and Grey and Reid (1975). Samples of chloride-free titanium oxide and amorphous coprecipitates of iron and titanium hydrated oxides were prepared using the methods described by Fitzpatrick *et al.* (1978).

The hydrothermal experiments were carried out at 2.2 kbar in a water-cooled, cold-seal 5 cm diameter Nimonic 105 steel bomb similar to that described by Luth and Tuttle (1963). Pressure was supplied by a hand-operated hydraulic water intensifier and measured using a stainless-steel bourdon gauge. The bomb was heated by a nichrome wire electric furnace inclined at 20° to the horizontal. Temperatures were measured with a steel-sheathed chromel-alumel thermocouple positioned inside the bomb, 4 cm from the bottom of the axial hole. A stainless-steel filler rod was used to reduce thermal gradients along the axis of the vessel (Boettcher and Kerrick, 1971).

For the hydrothermal runs, about 150 mg of the freshly coprecipitated iron and titanium oxides were mixed with 1–1.5 ml of ammonium nitrate solution, pH 5–6, and sealed in 6 × 50 mm gold capsules. Run times varied from 20 hr to 3 weeks but most runs were for 65 hr. At the completion of each run the pressure vessel was withdrawn from the furnace and cooled rapidly with compressed air. The reaction pressure was maintained until the bomb had cooled to ambient temperature.

Some aging experiments were also carried out at ambient pressure and temperatures of 70 and 90°C. The coprecipitates were aged at pH 4.5 and 6 for periods of 10–70 days using the procedure described by Fitzpatrick *et al.* (1978).

Thermal analysis experiments were performed using a Stanton Redcroft STA-780 Simultaneous Thermal Analyser, designed to give simultaneous thermogravimetric, differential thermogravimetric (DTG) and differential thermal analysis (DTA) curves. Sample weights of 20–30 mg were used and alumina was used as the reference material. All runs were carried out under a static air atmosphere. The samples were heated in platinum cups to 950°C at a rate of 10° min^{-1}. For the DTA curves, a sensitivity of 20 μV full-scale deflection was used. This high sensitivity was necessary to record the weak thermal effects associated with various dehydroxylation reactions, but it resulted in highly curved base lines (see Fig. 2(e,f)).

Room-temperature powder XRD patterns were recorded using a Philips diffractometer fitted with a graphite monochromator and employing Cu$K\alpha$ radiation. For the determination of lattice parameters, silicon was added as an internal standard and a scan rate of 0.25° (2θ) min^{-1} was used.

High-temperature diffractograms were recorded using a Rigaku theta–theta wide-angle goniometer fitted with a high-temperature X-ray diffractometer attachment and automatic temperature programmer. A sample was heated to a particular temperature and the diffractogram recorded immediately (Cu$K\alpha$ radiation, scan rate = 0.5° (2θ) min^{-1}). The sample was then held at temperature and diffractograms were recorded at 2-hourly intervals through the day and then again after an overnight equilibration. The temperature was then increased by 100°C and the procedure repeated, up to a maximum temperature of 1000°C. Deviations from this procedure occurred occasionally when the temperature was set to correspond to a particular DTA/DTG event.

A number of samples were chemically analysed for total iron and titanium. No significant deviation occurred from the Ti/(Ti+Fe) ratios in the original mixed solutions used for coprecipitation.

Experimental results

Hydrothermal synthesis

The results of the hydrothermal experiments are summarized in Figure 1. The area outlined delineates the composition-temperature regime for the formation of single-phase materials with XRD patterns resembling those of natural pseudorutile (Grey and Reid, 1975, Fig. 1). Single-phase products were obtained for compositions with $0.3 \leq Ti/(Ti+Fe) \leq 0.6$. The stability region shifts to higher temperatures as the TiO_2 content increases, from a mean value of 170°C at the lower limit to a mean value of 250°C at Ti/(Ti+Fe) = 0.6. At temperatures below the single-phase stability region, anatase always formed as a second phase whereas at higher temperatures partial decomposition to hematite and titanium oxide occurred. The titanium oxide was observed to be anatase below about 230°C, rutile above about 260°C and mixtures of the two for $230 < T < 260$°C.

Compositions with Ti/(Ti+Fe) < 0.3 gave mixtures of hematite, minor goethite and pseudorutile. We confirmed the observation of Fitzpatrick *et al.* (1978) that the single-phase pseudorutile region extends down to Ti/(Ti+Fe) = 0.2 at ambient pressure and 70°C. Compositions with Ti/(Ti+Fe) > 0.6 gave mixtures of pseudorutile and titanium oxides.

The stability region had a finite temperature width of about 30°C over the composition range. The field might actually be narrower, due to the difficulty of recognizing low concentrations of poorly crystallized anatase and/or hematite in the XRD patterns.

DTA/DTG analyses

Differential thermal analysis (DTA) patterns for four representative single-phase compositions with Ti/(Ti+Fe) = 0.3, 0.4, 0.5 and 0.6 are illustrated in Figure 2. The patterns display a similar array of three main endothermic peaks at ~50, 260 and 370°C, as well as shoulders near 170 and 320°C. Also given in Figure 2 is the DTA curve for natural pseudorutile. It displays an exothermic peak at 312°C as well as a well defined endothermic peak at 490°C and a very weak endotherm due to hygroscopic water at

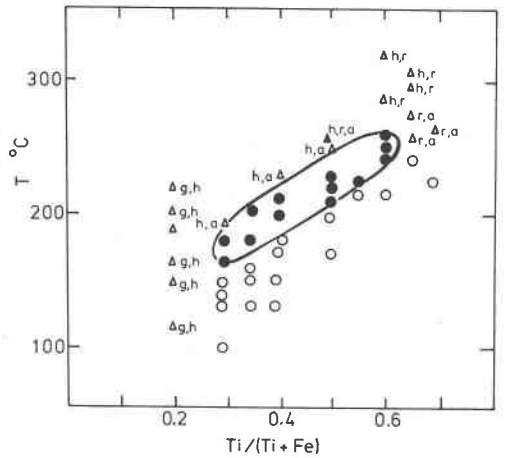

Fig. 1. Results of hydrothermal crystallization of mixed iron and titanium oxide coprecipitates. Filled circles—single-phase, goethite–rutile intergrowth (g–r). Open circles—two phases, g–r + anatase. Triangles—three-phase regions. Phases associated with g–r intergrowths are indicated by letters; a—anatase, g—goethite, h—hematite, r—rutile.

43°C. We also obtained thermal analysis patterns for altered ilmenites containing pseudorutile. They gave very similar DTA curves to that for the Neptune Island pseudorutile, with endothermic peaks in the range 480–530°C.

Differential thermogravimetric (DTG) curves for the synthetic samples are compared in Figure 3 with those for pseudorutile and goethite. The curves for the synthetic samples are very similar and resemble that for goethite. They comprise a peak due to loss of hygroscopic water near 50°C and a much larger asymmetric peak, for which the position increases with increasing Ti/(Ti+Fe) from 316°C (0.3) to 355°C (0.6). A shoulder is evident on the low-temperature side of the main peak (~260–280°C) for the synthetic samples.

For the natural pseudorutile sample, the main weight-loss peak moves to 490°C, consistent with the DTA curve. A small weight-loss peak due to hygroscopic water occurs near 50°C and a weak subsidiary peak occurs near 300°C. For the altered ilmenite samples, two weight-loss peaks near 300 and 500°C were also observed but they were of approximately equal intensity.

In Table 1 the measured total weight losses from the TG curves are given for all samples. From the areas under the DTG curves the relative weight losses due to hygroscopic and bound water have been determined and are given in Table 1.

X-ray diffraction

Typical X-ray diffractograms for synthetic samples with Ti/(Ti+Fe) = 0.3 and 0.6 are compared with the pattern for natural pseudorutile in Figure 4. The XRD patterns show relatively sharp peaks, labelled *s*, together with much broader peaks, labelled *m*, in Figure 4(a). The former reflections may be indexed using a hexagonal

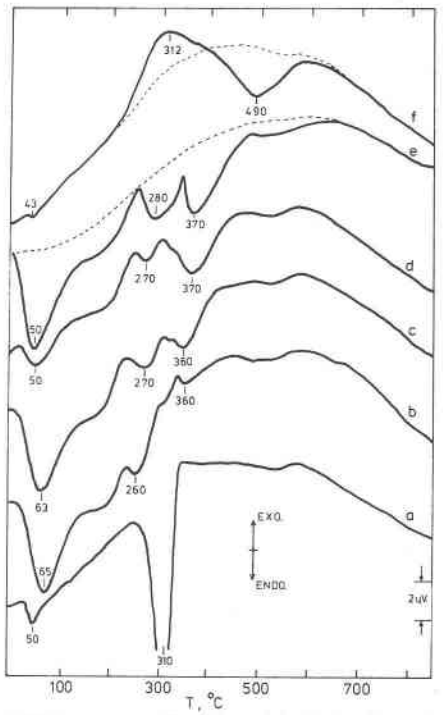

Fig. 2. DTA curves. Goethite, (a); hydrothermal reaction products with Ti/(Ti+Fe) = 0.3, (b); 0.4, (c); 0.5, (d); 0.6, (e); South Australian pseudorutile, (f). The dashed lines in (e) and (f) are baselines obtained by re-running the DTA curves for the samples after dehydration.

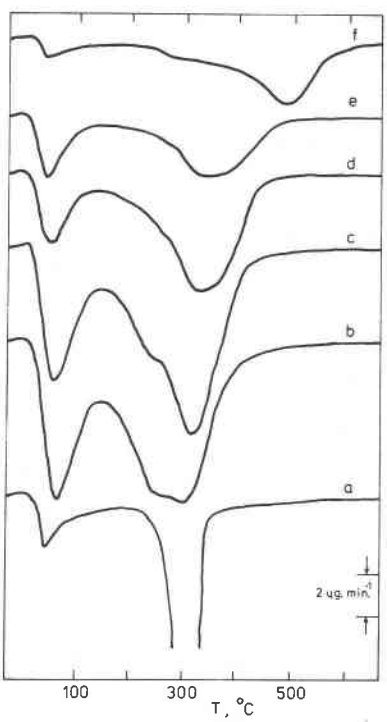

Fig. 3. DTG curves. Goethite, (a); hydrothermal reaction products with Ti/(Ti+Fe) = 0.3, (b); 0.4, (c); 0.5, (d); 0.6, (e); South Australian pseudorutile, (f).

Table 1. Differential thermogravimetric (DTG) results

Ti/(Ti + Fe)	DTG peaks (°C)	Measured weight loss (wt.%)			
		Total	Hygroscopic water	Structural water	Calculated for $(FeOOH)_{2p}(TiO_2)_q$
0.3	51, 269(sh), 316	7.1	1.6	5.5	7.3
0.4	63, 261(sh), 321	6.6	1.2	5.4	6.3
0.5	51, 280(sh), 342	5.2	0.8	4.4	5.3
0.6	50, 279(sh), 355	4.9	0.9	4.0	4.3
0.62 (pseudorutile)	52, 275(sh), 490	3.2	0.3	2.9	4.1

subcell with $a_h \simeq 2.9$Å, $c_h \simeq 4.6$Å, which corresponds to the unit cell for a hexagonal closest-packed array of anions (Teufer and Temple, 1966), whereas the latter are superlattice reflections due to metal atom ordering (Grey and Reid, 1975). Lattice parameters obtained by least squares refinement of the 2θ values for the subcell peaks are given in Table 2. With increasing Ti/(Ti+Fe) ratios, there is a contraction of both a_h, and c_h. Also given in Table 2 are the positions of the two major peaks due to metal-ordering at $2\theta \simeq 23°$ and 33°. With decreasing Ti/(Ti+Fe) ratios, the peak at $2\theta \simeq 23°$ moves to lower angles and that at $2\theta \simeq 33°$ moves to higher angles.

The mean crystalline dimension (MCD, *i.e.*, a measure of the size of the domains of ordered structure) was calculated from measurements of XRD line broadening for both the anion sublattice reflections and the metal-ordering reflections.[1] The former gave MCD values that decreased with decreasing Ti content from 100Å, Ti/(Ti+Fe) = 0.6 to 80Å, Ti/(Ti+Fe) = 0.3. The MCD values obtained from the metal-ordering reflections were much lower, typically 40–50Å. For pseudorutile, the MCD value corresponding to metal ordering was slightly lower than that obtained for the synthetic phases, whereas the anion-lattice MCD was 160Å, indicating a larger domain size in the natural mineral.

XRD patterns were recorded also for the DTA residues (heated to 950°C). Samples with Ti/(Ti+Fe) < 0.5 gave pseudobrookite, Fe_2TiO_5, or mixtures of pseudobrookite and hematite. By contrast, XRD patterns for samples with Ti/(Ti+Fe) ≥ 0.5 showed lines due only to a member of the $Fe_2Ti_2O_7$–$Fe_2Ti_3O_9$ homologous series (Grey and Reid, 1972). The XRD pattern for the DTA residue of the natural pseudorutile also showed this phase, together with some rutile.

The changes resulting from heating the phases in air were examined in more detail for the Ti/(Ti+Fe) = 0.3 and 0.5 compositions, using a high-temperature X-ray diffractometer. For the former phase, no significant change in the XRD patterns was observed up to a temperature of 360°C, at which very broad peaks due to hematite appeared. Between 360 and 600°C, the pseudorutile-like phase disappeared and the hematite peaks sharpened. At 600°C, broad peaks due to rutile apeared and mixtures of rutile plus hematite persisted up to 725°C at which temperature pseudobrookite formed. Heating at higher temperatures resulted in a gradual disappearance of the rutile and hematite peaks and an increase and sharpening of the pseudobrookite peaks. At 900°C, pseudobrookite together with hematite were the only products.

For the composition with Ti/(Ti+Fe) = 0.5, no change to the pattern occurred up to 300°C, at which temperature the broad metal-ordering peak at $2\theta = 23°$ suffered a marked reduction in intensity. At 400°C this peak had virtually disappeared and the metal-ordering peak at $2\theta = 32°$ had also reduced in intensity. At 500°C the subcell reflections at $2\theta = 36°$ and 41° broadened and became asymmetric, and a shoulder appeared on the low-angle side of the $2\theta = 32°$ peak. These effects are the first signs of the formation of the $Fe_2Ti_{n-2}O_{2n-1}$ intergrowth phases (Grey and Reid, 1972). At 600°C, very broad weak peaks due to hematite appeared. With increasing temperature there was a gradual development of crystallinity of both the $Fe_2Ti_{n-2}O_{2n-1}$ intergrowth phase and hematite. At 850°C, the reaction product comprised dominant $Fe_2Ti_{n-2}O_{2n-1}$, n = 3, *i.e.*, the high-temperature form of $Fe_2Ti_3O_9$, together with a small amount of hematite. This phase assemblage was unstable relative to pseudobrookite above 900°C.

High-temperature diffractograms were also recorded for natural pseudorutile. The changes in the diffractograms with increasing temperature were similar to those for the synthetic phase with Ti/(Ti+Fe) = 0.5. The main difference was a sharpening of the metal-ordering peaks as the temperature was increased up to ~370°C. This ordering process is manifested as a broad exothermic peak in the DTA pattern (see Fig. 2(f)). A second difference was that hematite did not form with the $Fe_2Ti_3O_9$ intergrowth phase.

Discussion

Thermal properties and compositions

For the synthetic phases the DTG curves are clearly resolved into two peaks corresponding to hygroscopic

[1] MCD = $0.9\lambda/B\cos\theta$, $B = (B_m^2 - B_i^2)^{1/2}$ where B_m = measured width at half height and B_i = instrumental line broadening (Cullity, 1959).

Table 2. Crystallographic data

Ti/(Ti + Fe)	Subcell parameters		Metal-ordering reflections, 2θ (°)	
	a (Å)	c (Å)	2θ Observed	Calculated for $(FeOOH)_{2p}(TiO_2)_q$
0.2[a]	2.924(2)	4.627(8)	21.8	21.5 p = 2, q = 1
			33.4	34.3[b] (35.3, 33.3)
0.3	2.905(3)	4.620(5)	22.2	21.9 p = 1, q = 1
			33.0	33.6 (33.6, 33.6)
0.4	2.904(2)	4.605(3)	22.4	22.2 p = 3, q = 4
			32.8	33.3 (32.8, 33.8)
0.5	2.892(2)	4.585(4)	23.0	22.7 p = 1, q = 2
			32.6	32.8 (31.6, 34.1)
0.6	2.879(3)	4.582(6)	23.2	23.2 p = 1, q = 3
			32.1	32.4 (30.5, 34.4)
S.A. pseudorutile 0.62	2.868(3)	4.607(5)	23.0	
			32.3	
Tivanite 0.44	2.881	4.552	22.92	
			32.02, 34.01	

[a]Prepared at 70°C, 1 bar.

[b]Average of the positions of the two reflections given in parentheses.

water (~50°C) and structurally bound water (~300–400°C) respectively. For all samples the structural water (hydroxyls) represents the major weight loss component and it increases with increasing iron content. The DTG curves resemble that for goethite, (FeOOH), and in Table 1 the measured structural water contents are compared with values calculated for FeOOH–TiO_2 mixtures. The measured values are lower than the calculated values by 10–20 percent. If we assign all the structurally bound water to hydroxyls, then the calculated compositions for the phases with Ti/(Ti+Fe) = 0.3 and 0.6 are $Fe_{0.70}Ti_{0.30}O_{1.38}(OH)_{0.54}(H_2O)_{0.08}$ and $Fe_{0.40}Ti_{0.60}O_{1.61}(OH)_{0.38}(H_2O)_{0.04}$ and the anion-to-cation ratios are 1.92 and 1.99 respectively, compared with a value of 2.00 for goethite–rutile mixtures.

The numerous endotherms spread over a wide temperature range in the DTA curves and the broad DTG peaks are consistent with the observed small domain size of the ordered regions in the synthetic phases. As reported above, measurement of line broadening in the X-ray patterns gave MCD's in the range 50–100Å. When the ordered domains are so small, surface and near-surface hydroxyls represent a significant proportion of the total hydroxyl content, and if the dehydroxylation is diffusion-controlled, as occurs in goethite (MacKenzie and Berggren, 1970), hydroxyl will be lost over a range of temperatures.

The complexity of the thermal analysis curves must in part also be due to variations in the local ordering of titanium and iron atoms. We tentatively assign the peaks near 270 and 360°C to loss of hydroxyls from iron-rich and titanium-rich (or simply titanium-containing) composition regions respectively, *i.e.*, the energy of bonding of hydroxyls to Ti^{4+} is expected to be higher than that to Fe^{3+}.

For pseudorutile, the main DTA/DTG peak is displaced to a higher temperature by ~100°C, *cf.* the synthetic phase with similar composition, Ti/(Ti+Fe) = 0.6. This is most likely due to the higher degree of crystallinity of the natural material. As discussed above, in going from the synthetic phases to the mineral, there is a doubling of the mean crystallite diameter from 80–100Å to 160Å, which corresponds to an ~8-fold increase in the domain volume and this is expected to have a considerable effect on the dehydroxylation processes, particularly if they are diffusion controlled.

As indicated in Table 1, the weight loss in pseudorutile due to dehydroxylation, 2.9 wt.%, is considerably lower than the theoretical value of 4.1 wt.% for a goethite–rutile intergrowth with Ti/(Ti+Fe) = 0.62. Combining the thermal analysis data and chemical analyses (Grey and Reid, 1975), the formula for South Australian pseudorutile, normalized to 5 cations, may be given as

$$Fe^{3+}_{1.81}Fe^{2+}_{0.07}Mn^{2+}_{0.03}Ti_{3.09}O_{8.33}(OH)_{1.33}(H_2O)_{0.07}$$

The anion-to-metal ratio for the oxyhydroxide mineral is 1.93; *cf.* a ratio of 1.80 for the theoretical oxide composition often ascribed to pseudorutile, $Fe_2Ti_3O_9$, and a ratio of 2.00 for an ordered goethite–rutile intergrowth, $(FeOOH)_2(TiO_2)_3$.

Structure models

Pseudorutile. Precession and Weissenberg photographs for individual grains of natural pseudorutile display patterns characteristic of single crystals (Teufer and Temple, 1966). The patterns show relatively sharp, well defined spots that can be indexed by a simple hexagonal cell, a = 2.87Å, c = 4.61Å, as well as diffuse streaks, or arcs, due to metal-atom ordering (Grey and Reid, 1975). The metal-ordering diffuse streaks are confined to recip-

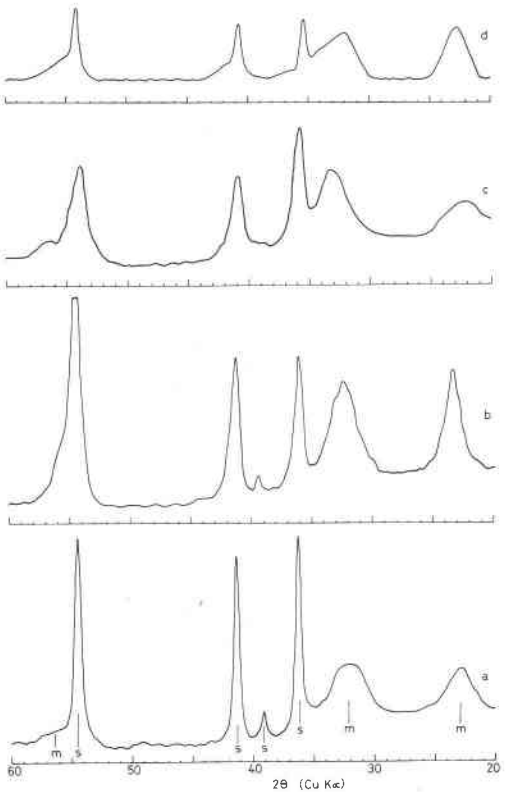

Fig. 4. X-ray powder diffraction patterns. (a) South Australian pseudorutile. Anion lattice subcell reflections are labelled *s* and metal-ordering superlattice reflections are labelled *m*, (b) synthetic phase with Ti/(Ti+Fe) = 0.6, (c) synthetic phase with Ti/(Ti+Fe) = 0.3, (d) calculated pattern for tivanite (Grey and Nickel, 1981) using POWGEN (Stewart, 1976) with FWHH parameters of 0.5° (2θ) for the subcell peaks and 2° for the metal-ordering reflections.

rocal layers of the hexagonal cell with l odd and are incommensurate with the subcell reciprocal lattice. We have previously established a model for the short-range ordering of the metal atoms in pseudorutile in the approximation of a commensurate hexagonal superlattice with $a = 5a_{\text{subcell}}$ (Grey and Reid, 1975). The model gave a satisfactory account of the distribution of the intensities of the metal-ordering reflections, with the streaks approximated as Bragg peaks, but gave no information on the geometry of the diffuse diffraction effects.

An insight into the origin of the shape of the diffuse reflections comes from a study of the mineral tivanite, which is an ordered intergrowth of goethite-type and rutile-type structures (Grey and Nickel, 1981). The structure of this mineral was determined on a multiply twinned crystal fragment and it was observed that the diffraction patterns for twinned tivanite and pseudorutile were very similar, with the reflections from the various twin individuals of tivanite lying on curves or arcs corresponding closely, in extent and orientation, to the diffuse reflections in pseudorutile. This is illustrated in Figure 5 in which an (hk1) precession photograph for pseudorutile is compared with a schematic representation of the ($h1l$) reciprocal section for multiply twinned tivanite in which the twin laws correspond to the various symmetry elements of the hexagonal anion sublattice. The close agreement between the patterns leads us to propose that the structure of pseudorutile comprises a statistical distribution of the various possible twin variants of a goethite–rutile intergrowth structure in microdomains of average dimension 40–50Å. The coherency of the hexagonal close-packed anion framework is maintained over 3–4 twin variants on average (~160Å). The broadening of the diffraction spots due to the very small domain size results in a coalescence of neighbouring reflections from different twin variants, producing arcs or streaks of diffracted intensity, as experimentally observed.

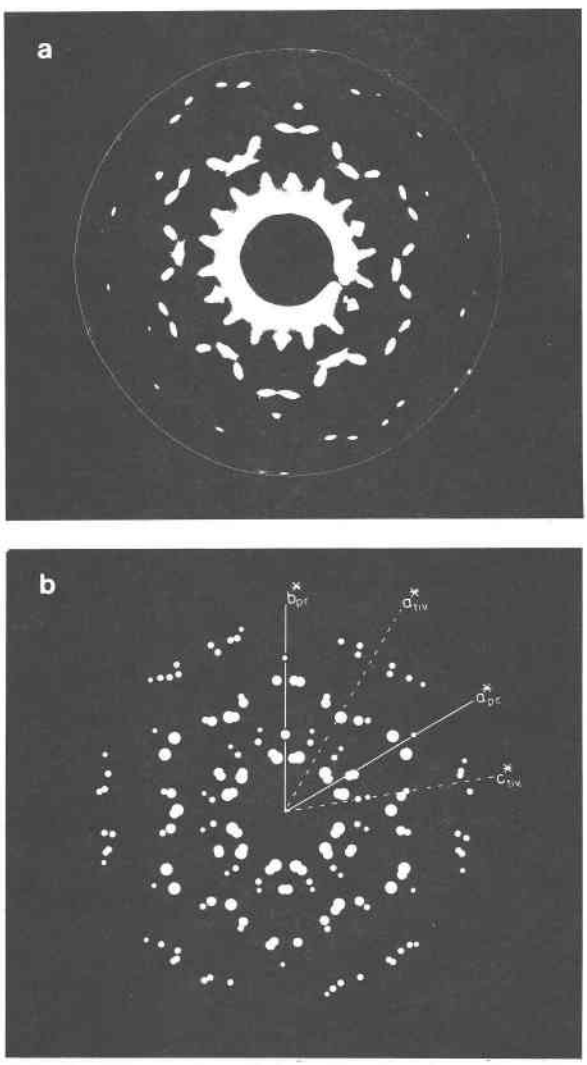

Fig. 5. (a) Precession photograph of (hk1) level for natural pseudorutile. (b) Schematic representation of the ($h1l$) level for twinned tivanite. The areas of the circles are proportional to F^2.

Synthetic phases. The powder XRD patterns for the synthetic phases are very similar to those for pseudorutile and tivanite, Figure 4 and Table 2, suggesting that their structures are closely related and based on unit-cell intergrowths of goethite-type and rutile-type substructures.

We have previously noted that the goethite structure may be formally derived from the rutile structure (or vice versa) by the application of the antiphase operation $1/2[013](0\bar{3}1)_{\text{rutile}}$ to every second $(0\bar{3}1)_{\text{rutile}}$ plane (Grey and Nickel, 1981). It follows that, in principle, an infinite number of ordered intergrowth phases comprising different width slabs of goethite and rutile type, spanning the full range of Ti/(Ti+Fe) may be formed simply by changing the periodicity of the antiphase boundaries. Inspection of the structural models leads to relationships between the unit cell vectors of the intergrowth phases, with composition expressed as $(FeOOH)_{2p}(TiO_2)_q$, p and q integers, and those of the rutile parent structure, given by the matrix:

$$\begin{matrix}\mathbf{a}\\ \mathbf{b}\\ \mathbf{c}\end{matrix} = \begin{bmatrix} 0 & \frac{2+p}{2} & 3-\frac{p}{2}-q \\ 1 & 0 & 0 \\ 0 & -1 & -3 \end{bmatrix} \begin{matrix} a_r \\ b_r \\ c_r \end{matrix}$$

Examples of intergrowth structures corresponding to the compositional extremes encountered for the synthetic samples (Ti/(Ti+Fe) = 0.2 and 0.6) are illustrated in Figure 6.

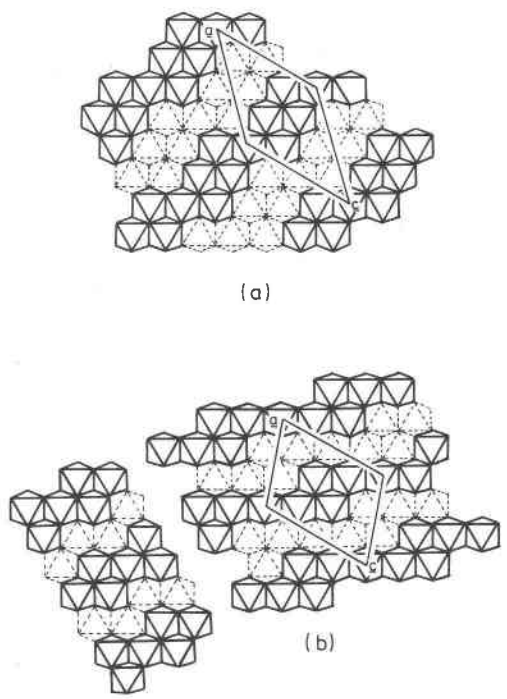

Fig. 6. Polyhedral representation of goethite–rutile intergrowths $(FeOOH)_{2p}(TiO_2)_q$. (a) p = 2, q = 1; (b) p = 1, q = 3 is shown on the right. The structure of its dehydroxylation product, $Fe_2Ti_3O_9$ (Grey *et al.*, 1973) is shown on the left.

The above equations may be used to calculate the Miller Indices of the superlattice reflections and thus to calculate *d*-spacings, or 2θ values. We have calculated 2θ values for the low-angle metal-ordering reflections for selected intergrowths and these are compared with the measured values in Table 2. The close agreement between the two sets of values lends support to the above intergrowth model. For the reactions carried out at 2 kbar, the broad metal-ordering peak at $2\theta \simeq 32°$ is not resolved into two reflections as occurs for the ordered intergrowth in tivanite (Table 2) and it is concluded that in the 2 kbar hydrothermal products the metal ordering is very short-range in nature, consistent with the measured MCD values of only 40–50Å.

The intergrowth models, illustrated in Figure 6, provide an explanation for the observed phase changes resulting from heating the synthetic phases. As noted above, phases with Ti/(Ti+Fe) $\gtrsim$ 0.5 reacted to form $Fe_2Ti_{n-2}O_{2n-1}$ homologues at temperatures below 900°C, whereas phases with lower titanium contents dissociated into hematite plus rutile. In Figure 6(b), the structure of the goethite–rutile intergrowth phase with Ti/(Ti+Fe) = 0.6, $Fe_2Ti_3O_8(OH)_2$, is compared with the structure of $Fe_2Ti_3O_9$ (Grey *et al.*, 1973) which is its dehydroxylation product. It is seen that the structures are closely related and exhibit the same periodicity between chains of metal atoms. Only a small number of cation diffusive hops are needed to transform one structure into the other in microdomains of ~50–100Å. If dehydroxylation of $Fe_2Ti_3O_8(OH)_2$ proceeds by an inhomogeneous mechanism, as proposed for brucite (Ball and Taylor, 1961) and goethite (Lima de Faria, 1963), then the local charge imbalance produced by the diffusion of protons can be simply redressed by diffusion of a relatively small number of cations from donor to acceptor regions to form $Fe_2Ti_3O_9$. Although this is a metastable phase in the Fe_2O_3–TiO_2 system, its formation is expected to be energetically favored over the large-scale diffusion of cations needed to produce segregated regions of hematite and rutile. By contrast with the above situation where there are similar amounts of Ti and Fe, the synthetic phases with low Ti/(Fe+Ti) contain extended regions of goethite-structure in which iron is expected to be ordered, *e.g.*, as shown for $Fe_4TiO_6(OH)_4$ in Figure 6(a). On dehydroxylation, these regions will form nuclei for hematite formation and growth, as experimentally observed.

The simple structural models based on rutile–goethite intergrowths need to be modified to take into account the measured anion-to-metal ratio which is less than 2 for both the synthetic phases and pseudorutile. If the metal atoms are restricted to octahedral sites in the closest-packed anion framework, this necessitates sharing of octahedral faces, resulting in the formation of local re-

gions of disordered hematite-like structure. This, or some other type of metal-rich structure, may form at the domain boundaries (*i.e.*, twin boundaries for the metal-ordering). Alternatively, non-stoichoimetry on the micro-domain surface may play an important role in determining the bulk composition. The elucidation of these finer structural details requires more detailed studies including techniques such as high-resolution electron microscopy and convergent-beam electron diffraction to determine the symmetry in individual domains.

Acknowledgments

We wish to thank Mr. I. Madsen for running the high-temperature diffractograms and Ms. I. Palmer for chemically analyzing the coprecipitated oxide samples. We thank also Dr. J. Hamilton for making available his DTA/DTG apparatus.

References

Ball, M. C. and Taylor, H. F. W. (1961). The dehydration of brucite. Mineralogical Magazine, 32, 754–766.

Boettcher, A. L. and Kerrick, D. M. (1971). Temperature calibration in cold-seal pressure vessels. In Gene C. Ulmer, Ed., Research Techniques for High Pressure and High Temperature, p. 179–193. Springer-Verlag, New York.

Cullity, B. D. (1959). Elements of X-ray Diffractions. Addison-Wesley, Reading, U.S.A.

Dyadchenko, M. G. and Khatuntseva, A. Ya. (1960). Mineralogy and geochemistry of the weathering process in ilmenite. Doklady Akademii Nauk SSSR, 132, 435–438.

Ernst, T. (1943). Fusion equilibria in the system Fe_2O_3–FeO–TiO_2 and remarks on the minerals pseudobrookite and arizonite. Zeitschrift für Angewandte Mineralogie, 4, 394–409.

Fitzpatrick, R. W., Le Roux, J. and Schwertmann, U. (1978). Amorphous and crystalline titanium and iron–titanium oxides in synthetic preparations, at near ambient conditions, and in soil clays. Clays and Clay Minerals, 26, 189–201.

Gevorkyan, V. Kh. and Tananayev, N. V. (1964). Some data on the initial stages of leucoxenization of ilmenite from the sedimentary deposits of the northern Azov area. Dopovidi Akademii Nauk Ukrains 'Koi RSR, 10, 1366–1369.

Gmelin (1932). Handbuch der Anorganischem Chemie. Eisen, Teil B, System number 59, p. 1128. Verlag Chemie, Berlin.

Grey, I. E. and Reid, A. F. (1972). Shear structure compounds $(Cr,Fe)_2Ti_{n-2}O_{2n-1}$ derived from the α-PbO_2 structural type. Journal of Solid State Chemistry, 4, 186–194.

Grey, I. E. and Reid, A. F. (1975). The structure of pseudorutile and its role in the natural alteration of pseudorutile. American Mineralogist, 60, 898–906.

Grey, I. E. and Nickel, E. H. (1981). Tivanite, a new oxyhydroxide mineral from Western Australia, and its structural relationship to rutile and diaspore. American Mineralogist, 66, 866–871.

Grey, I. E., Reid, A. F. and Allpress, J. G. (1973). Compounds in the system Cr_2O_3–Fe_2O_3–TiO_2–ZrO_2 based on intergrowth of the α-PbO_2 and V_3O_5 structural types. Journal of Solid State Chemistry, 8, 86–99.

Karkhanavala, M. D. and Momin, A. C. (1959). Subsolidus reactions in the system Fe_2O_3–TiO_2. Journal of the American Ceramic Society, 42, 399–402.

Larrett, M. J. W. and Spencer, W. G. (1971). Contributions to Australasian mineralogy: 3 'Pseudorutile' from South Neptune Island, South Australia. Amdel Bulletin, 12, 74–80.

Lima de Faria, J. (1963). Dehydration of goethite and diaspore. Zeitschrift für Kristallographie. Kristallgeometrie, Kristallphysik, Kristallchemie, 119, 176–203.

Luth, W. C. and Tuttle, O. F. (1963). Externally heated cold-seal pressure vessels for use to 10,000 bar and 750°C. American Mineralogist, 48, 1401–1403.

MacKenzie, R. C. and Berggren, G. (1970) Oxides and hydroxides of higher-valency elements. In R. C. MacKenzie, Ed., Differential Thermal Analysis, Vol. 1, p. 272–302. Academic Press, London.

Palmer, C. (1909). Arizonite, ferric metatitanate. American Journal of Science, 28, 353–356.

Pesce, B. (1931). Iron titanates. Gazzetta Chimica Italiana, 61, 107–111.

Stewart, J. M., Ed. (1976). The XRAY system—version of 1976. Computer Science Center, University of Maryland, TR-446.

Temple, A. K. (1966). Alteration of ilmenite. Economic Geology, 61, 695–714.

Teufer, G. and Temple, A. K. (1966). Pseudorutile—a new mineral intermediate between ilmenite and rutile in the natural alteration of ilmenite. Nature (London), 211, 179–181.

Manuscript received, August 11, 1982;
accepted for publication, March 18, 1983.